

# diffusion-fundamentals

The Open-Access Journal for the Basic Principles of Diffusion Theory, Experiment and Application

## Oxygen Diffusion in Oxide Crystals - Tracing New Routes to Identify the Rate Limiting Step of Oxygen Permeation through Perovskite Membranes

Haihui Wang<sup>1</sup>, Weishen Yang<sup>2</sup>, Cristina Tablet<sup>1</sup>, Jürgen Caro<sup>1</sup>

<sup>1</sup>Institute of Physical Chemistry and Electrochemistry, University of Hanover, Germany

<sup>2</sup> State Key Laboratory of Catalysis, Dalian Institute of Chemical Physics, China

Corresponding author:

Dr. Haihui Wang

Institute of Physical Chemistry and Electrochemistry

University of Hanover

Callinstr. 3-3A, D-30167 Hanover, Germany

Tel.: +49-511-7623080; Fax: +49-511-76219121

E-mail address: [Haihui.Wang@pci.uni-hannover.de](mailto:Haihui.Wang@pci.uni-hannover.de)

### Abstract

Perovskites are known as mixed electric conductors because they show both electronic (via electron holes) and ionic (via oxygen vacancies) conductivity. Since the electron conductivity is orders of magnitude higher than the ionic one, oxygen vacancy bulk diffusion is regarded as the rate limiting step in oxygen permeation through perovskites. However, for thin perovskite layer the rate of this bulk diffusion process starts to compete with the so called surface reaction which represents the dissociative adsorption and desorption of the oxygen molecule and the incorporation/release of the oxygen ions from the perovskite framework. The oxygen permeation flux through the perovskite membrane made of  $\text{Ba}_{0.5}\text{Sr}_{0.5}\text{Co}_{0.8}\text{Fe}_{0.2}\text{O}_{3-\delta}$  (BSCF) has been measured as a function of both the temperature, membrane thickness and the oxygen pressure gradient across the membrane. A combined bulk diffusion/surface reaction model can be used to understand the mechanism of the oxygen transport. The limiting step of the oxygen transport was found to be the bulk oxygen ion diffusion coefficient ( $D_i$ ) for the BSCF perovskite at temperatures above 700 °C. Furthermore, the oxygen vacancy diffusion coefficient ( $D_v$ ) can be deduced from the dependence of the oxygen permeation flux on the oxygen pressure gradient provided that the oxygen vacancy  $\delta$  are known. From permeation measurement on the BSCF membrane tube under study,  $D_v$  is found to be between  $2.82 \times 10^{-5} \text{ cm}^2/\text{s}$  at 900 °C and  $0.82 \times 10^{-5} \text{ cm}^2/\text{s}$  at 700 °C.

**Keywords:** Perovskite, oxygen diffusion, oxygen permeation

## 1. Introduction

Perovskites ( $\text{ABO}_3$ ) are a prominent topic of research in materials science (high- $T_c$ -electric conductor [1, 2], ferroelectric [3, 4] or high  $k$  dielectric [5], or magnetoresistance [6] material). Doping of these perovskites with multivalent cations on the A- and B-sites can lead to the simultaneous occurrence of ionic and electronic conductivities. For example, the partial substitution of Sr and Co for La and Fe in the A- and B-sites of  $\text{LaFeO}_3$  can result in a mixed conductor because oxygen vacancy ( $\delta$ ) are formed at the elevated temperature [7]. In recent years, such perovskite-type membranes with mixed ionic and electronic conductivities are of interest not only for a simple oxygen separation [8], but also for their potential use in the membrane reactor for the conversion of hydrocarbons, such as the partial oxidation of methane to syngas ( $\text{CO} + \text{H}_2$ ) [9 -12], the oxidative dehydrogenation of alkanes to alkenes [13 -17], and the oxidative methane to  $\text{C}_{2+}$  alkanes and alkenes [18, 19].

The oxygen permeation flux can be increased by reducing the thickness of the membrane, until its thickness becomes less than a characteristic value,  $d_c$ , at which the oxygen transport is equally limited by both the surface exchange kinetics and the bulk diffusion. Below  $d_c$ , a further decrease of the membrane thickness does not result in a remarkable increase of the oxygen permeation flux.  $^{18}\text{O} - ^{16}\text{O}$  isotopic exchange techniques are usually used to measure the oxygen self-diffusion coefficient  $D_s$  and the surface exchange coefficient  $k_s$ , from which the limiting step of the oxygen transport can be determined. If the membrane thickness  $d \gg d_c$ , bulk transport is rate determining, for  $d \ll d_c$  the surface processes govern the overall rate. In the  $^{18}\text{O} - ^{16}\text{O}$  isotope tracer method, the  $^{18}\text{O}$  diffusion profile is studied by secondary ion mass spectrometry (SIMS) line scanning [20]. On the other hand, impedance spectroscopy detects not only the charge carrier mobility, but also it can be used to separate the resistances originating from the bulk and the grain boundaries by frequency variation because of the different time scales [21].

This overview is dedicated to the derivation of the rate limiting step of the oxygen transport in the perovskite membranes, as the basic for the expected application of oxygen transporting membrane in catalytic membrane reactors. For this, the oxygen vacancy diffusion coefficient ( $D_v$ ) was deduced from oxygen permeation measurements as a function of the oxygen pressure gradient and the membrane thickness. The system  $\text{Ba}_{0.5}\text{Sr}_{0.5}\text{Co}_{0.8}\text{Fe}_{0.2}\text{O}_{3-\delta}$  (BSCF) was chosen for this study because it is an excellent perovskite membrane which was widely studied for oxygen separation [8, 22] and as a membrane reactor for the partial oxidation of methane to synthesis gas [10, 12], and for the selective oxidation of light hydrocarbons [14, 16, 17].

## 2. Theory

Fig. 1 illustrates the oxygen permeation through a dense oxygen permeable membrane driven by an oxygen partial pressure gradient across it. The oxygen permeation involves three steps. At first, oxygen molecules adsorb and become reduced to oxygen ions at the membrane surface exposed to the high oxygen partial pressure,  $P'_{\text{O}_2}$ . Driven by the chemical potential gradient, oxygen ions and electrons counter

diffuse through the bulk of the membrane. Finally, oxygen molecules were formed by recombining oxygen ions at the membrane surface exposed to the low oxygen partial pressure,  $P_{O_2}''$  and release to gas phase. Local charge neutrality is maintained by the joint diffusion of oxygen vacancies and electrons or electron holes. The net flux is determined by the species with the smallest conductivity.

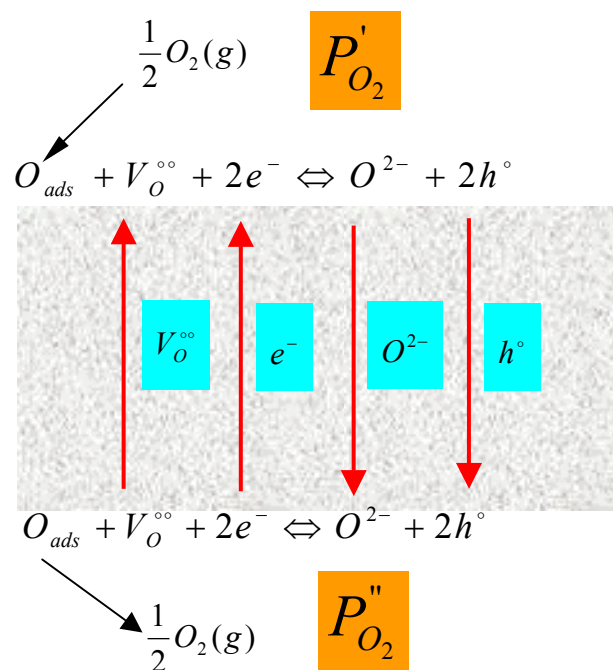


Fig. 1: Fluxes in mixed conducting membrane under a partial pressure gradient.

$P_{O_2}'$  is the higher oxygen partial pressure,  $P_{O_2}''$  is the lower oxygen partial pressure.

The oxygen permeation flux through the perovskite membranes is essentially controlled by two factors, by (i) the rate of the oxygen ion ( $O^{2-}$ ) / oxygen vacancy ( $V_O^{\circ\circ}$ ) diffusion and/or the simultaneous counter flux of the charge balancing electrons ( $e^-$ ) /electron holes ( $h^\circ$ ) within the bulk membrane and by (ii) the interfacial oxygen exchange on either side of the membrane, as shown in Fig. 2. Considering oxygen exchange between the gas phase and the oxide surface, one may distinguish many steps, like adsorption, dissociation, surface diffusion, charge transfer and incorporation in the surface layer, and reversed steps, each of these steps may impede interfacial transfer of oxygen. If the oxygen permeation is limited by the surface exchange, the oxygen permeation flux can be given:

$$j_{O_2} = k_0 c_0 \times \left( P_{O_2}'^{\frac{1}{2}} - P_{O_2,S}^{\frac{1}{2}} \right) \quad (1)$$

or

$$j_{O_2} = k_0 c_0 \times \left( P_{O_2,S}^{\frac{1}{2}} - P_{O_2}''^{\frac{1}{2}} \right) \quad (2)$$

where  $k_0$  is the surface exchange coefficient,  $c_0$  is the density of oxygen ions on the surface.

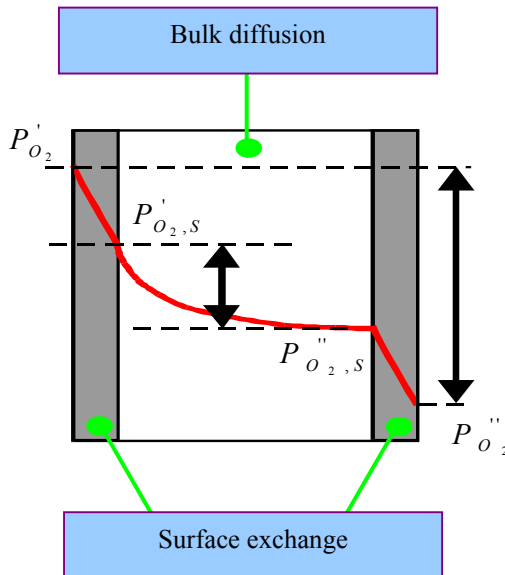


Fig. 2: Oxygen transport through both interfaces and bulk.

$P_{O_2,S}'$  and  $P_{O_2,S}''$  are the virtual oxygen pressure on the interfaces of feed side and permeate side.

For a thick membrane the rate of the overall oxygen permeation is usually determined by the lattice diffusion of oxygen or the transport of electronic charge carriers through the bulk oxide. The gradient  $\nabla\mu_{O_2}$  of the chemical potential of the oxygen on the two sides of the membrane is regarded as the driving force for the oxygen ion transport. Assuming ion diffusion in the bulk of the solid electrolyte as rate limiting, the oxygen potential gradient depends at a given temperature  $T$  and a membrane thickness  $d$  only on the oxygen partial pressures on the feed (air) and permeate side of the membrane,  $P_{O_2,S}'$  and  $P_{O_2,S}''$ , respectively [23]

$$\nabla \mu_{O_2} = \frac{\mu''_{O_2} - \mu'_{O_2}}{d} = \frac{RT}{d} \ln \left( \frac{P''_{O_2,S}}{P'_{O_2,S}} \right) \quad (3)$$

When the bulk diffusion is the limiting step of oxygen transport, it means that the surface reaction is so fast that a fast equilibration of the oxide surface with the imposed gas atmosphere would imply that  $P'_{O_2,S} = P'_{O_2}$  and  $P''_{O_2,S} = P''_{O_2}$ . Eq. (3) can be changed to:

$$\nabla \mu_{O_2} = \frac{\mu''_{O_2} - \mu'_{O_2}}{d} = \frac{RT}{d} \ln \left( \frac{P''_{O_2}}{P'_{O_2}} \right) \quad (4)$$

For charge neutrality reasons, oxygen ion transport in one direction is accompanied by electron transport in the opposite direction. Considering the ionic and electronic conductivities  $\sigma_i$  and  $\sigma_e$  we obtain for the oxygen flux  $j_{O_2}$  through the membrane with  $F$  as Faraday constant:

$$j_{O_2} = -\frac{1}{4^2 F^2} \frac{\sigma_i \cdot \sigma_e}{\sigma_i + \sigma_e} \cdot \nabla \mu_{O_2} \quad (5)$$

If the oxygen ion transport occurs via oxygen vacancies ( $V_O^{oo}$ ) and the electron transport via electron holes ( $h^\circ$ ), we have the case of the counter diffusion of  $V_O^{oo}$  and  $2h^\circ$ . Integration of Eq. (5) across the membrane thickness  $d$  using the relationship

$\nabla \mu_{O_2} = \frac{\partial RT \ln P_{O_2}}{\partial x}$  yields the Wagner equation in the usual form which has general validity for mixed conductors [24]

$$j_{O_2} = -\frac{RT}{4^2 F^2 d} \int_{\ln p'_{O_2}}^{\ln p''_{O_2}} \frac{\sigma_i \cdot \sigma_e}{\sigma_i + \sigma_e} \cdot d \ln P_{O_2} \quad (6)$$

In order to understand the roles of the surface exchange and bulk diffusion during the oxygen transport through the perovskite membrane, a surface exchange fluxes model was introduced. The exchange flux  $i_i$  at the perovskite membrane – gas interfaces at the inlet and outlet sides is given by [25, 26]:

$$i_i = k_{i,0} C_i (e^{n\mu_g / RT} - e^{2n\mu / RT}) \quad (7)$$

where  $k_{i,0}$  is the surface exchange coefficient,  $C_i$  is the density of oxygen ions,  $n$  is the reaction order at the interfaces,  $\mu$  is the chemical potential of the oxygen ions at the two interfaces, and  $\mu_g$  is the chemical potential of the gas

$$\mu_g = RT \ln(P / P_0) \quad (8)$$

where  $P$  is the gas pressure and the subscript 0 indicates the standard pressure of 1.0 atm.

At the interfaces, the following reaction occurs:



Thus the reaction order,  $n$ , at the interfaces is  $n = \frac{1}{2}$ . The exchange oxygen fluxes  $i_1$  and  $i_2$  at the perovskite membrane – gas interfaces at the inlet and outlet sides are given by:

$$i_1 = k_{i,0} C_i (e^{\mu_{1g}/2RT} - e^{\mu_1/RT}) \quad (10)$$

$$i_2 = k_{i,0} C_i (e^{\mu_2/RT} - e^{\mu_{2g}/2RT}) \quad (11)$$

On the other hand, the flux density is determined by the charge, conductivity and the gradient of the electrochemical potential. Therefore, the oxygen ionic flux  $i_i$  can be also described by [21]:

$$i_i = -\frac{\sigma_i}{2F} \frac{d\mu}{d\phi} \quad (12)$$

where  $\phi$  is the diameter of the membrane tube,  $\sigma_i$  is the oxygen ion conductivity.

The oxygen ion conductivity is also determined by the oxygen ion diffusion coefficient  $D_i$  and the oxygen ion concentration  $C_i$  in the perovskites [21]

$$\sigma_i = \frac{D_i}{RT} 4F^2 C_i \quad (13)$$

By combining Eqs. (12) and (13) we get the oxygen permeation flux  $j_{O_2}$ ,

$$j_{O_2} = \frac{i_i}{2F} = -\frac{\sigma_i}{4F^2} \frac{d\mu}{d\phi} = -\frac{D_i C_i}{RT} \frac{d\mu}{d\phi} \quad (14)$$

The normalized oxygen permeation flux  $j_{O_2}$  can be expressed as:

$$j_{O_2} = \frac{f}{\pi\phi L} \quad (15)$$

where  $L$  is the length of the membrane tube,  $\pi\phi L$  is the membrane surface,  $f$  is the total oxygen flux through the membrane.

By combining Eqs. (14) and (15) we can get:

$$-\frac{D_i C_i}{RT} \frac{d\mu}{d\phi} = f / \pi \phi L \quad (16)$$

Continuity of ion flux requires that the surface exchange fluxes and the oxygen permeation flux  $J_{O_2}$  at the two interfaces match:

$$f / \pi \phi_1 L = k_{i,0} C_i (e^{\mu_{1g}/2RT} - e^{\mu_1/RT}) \quad (17)$$

$$f / \pi \phi_2 L = k_{i,0} C_i (e^{\mu_2/RT} - e^{\mu_{2g}/2RT}) \quad (18)$$

Integrating of Eq. (16) yields:

$$\mu_2 - \mu_1 = \frac{RTf}{\pi C_i D_i L} \ln(\phi_2 / \phi_1) \quad (19)$$

where  $\phi_1$  and  $\phi_2$  are the inner and outer diameters of the membrane tube

The following relation can be obtained by eliminating  $\mu_1$  and  $\mu_2$  in Eqs. (17) – (19)

$$\frac{f}{\pi C_i D_i L} \ln(\phi_2 / \phi_1) = \ln \left( \frac{\sqrt{P_{O_2}' / P_0} - f / \pi \phi_2 L C_i k_{i,0}}{\sqrt{P_{O_2}'' / P_0} + f / \pi \phi_1 L C_i k_{i,0}} \right) \quad (20)$$

If the oxygen transport is limited by the surface exchange,  $\mu_1 \rightarrow \mu_2$ , so Eq. (20) reduces to:

$$f = \frac{\pi \phi_1 \phi_2 L C_i k_{i,0}}{\phi_1 + \phi_2} \left( \sqrt{P_{O_2}' / P_0} - \sqrt{P_{O_2}'' / P_0} \right) \quad (21)$$

On the other hand, if the oxygen transport is limited by the bulk diffusion  $\mu_1 \rightarrow \mu_{1g}/2$  and  $\mu_2 \rightarrow \mu_{2g}/2$ , so Eq. (20) changes to:

$$f = \frac{\pi L C_i D_i}{2 \ln(\phi_2 / \phi_1)} \ln(P_{O_2}' / P_{O_2}'') \quad (22)$$

The total oxygen flux can be expressed by:

$$f = J_{O_2} \times S \quad (23)$$

where  $J_{O_2}$  is the oxygen permeation flux measured in the experiment and  $S$  is the effective area of the membrane tube. If the oxygen transport is limited by the surface exchange at the interfaces, Eq. (21) gives:

$$J_{O_2} = \frac{\pi \phi_1 \phi_2 L C_i k_{i,0}}{S(\phi_1 + \phi_2)} \left( \sqrt{P_{O_2}' / P_0} - \sqrt{P_{O_2}'' / P_0} \right) \quad (24)$$

Eq. (24) predicts that the oxygen permeation flux ( $J_{O_2}$ , mol/cm<sup>2</sup>.s) should be proportional to the pressure term  $\left(\sqrt{P'_{O_2}/P_0} - \sqrt{P''_{O_2}/P_0}\right)$  if only the surface exchange is the limiting step of the oxygen transport.

On the other hand, if the oxygen transport is only limited by the bulk diffusion through the membrane, the oxygen permeation flux is given by the following formula:

$$J_{O_2} = \frac{\pi L C_i D_i}{2S \ln(\phi_2/\phi_1)} \ln\left(\frac{P'_{O_2}}{P''_{O_2}}\right) \quad (25)$$

Now the oxygen permeation flux,  $J_{O_2}$ , is proportional to  $\ln\left(\frac{P'_{O_2}}{P''_{O_2}}\right)$  if the limiting step is the bulk diffusion.

### 3. Experimental

In the studies we refer to, the BSCF oxide powder was synthesized by a combined citrate and EDTA complexing method [22]. The membrane tube was prepared by the plastic extrusion method [27]. The sintered membrane tube has an outer diameter of about 8.0 mm, an inner diameter of about 5.0 mm. The densities of the sintered tubular membranes were measured by the Archimedes method with ethanol. Only those membranes that had a relative density higher than 90% were used for the permeation study. A shell-and-tube permeation cell (permeator) was used for oxygen permeation, as shown in Fig. 3. The membrane tube, which was sealed with two quartz tubes ( $\varnothing = 17$  mm), served as the tube side. Another quartz tube ( $\varnothing = 29$  mm) served as the shell side of the permeator. A tubular furnace was used to heat the permeator. The temperature was controlled by a microprocessor temperature controller (Model Al-708, Xiamen Yuguang Electronics Technology Research Institute) within  $\pm 1$  K of the set points and monitored by a K-type thermocouple encased near the tube. The inlet gas flow rates were controlled by mass flow controllers (model D07-7A/ZM, Beijing Jianzhong Machine Factory, China). High purity helium (>99.999%) was used as a sweep gas on the tube side of the permeator. GC (HP6890) equipped with a 3m 5A molecular sieve column for the separation of O<sub>2</sub> and N<sub>2</sub> was connected to the exit of the tube side to determine the O<sub>2</sub> concentration.

The oxygen permeation through the BSCF membrane tube was studied for different combinations of temperatures and oxygen partial pressures on the shell side ( $P'_{O_2}$ ) and on the tube side ( $P''_{O_2}$ ). The total flow rate of a mixture of O<sub>2</sub> and N<sub>2</sub> on the shell side was 300 mL/min and different oxygen partial pressures ( $P'_{O_2}$ ) on the shell side can be obtained by adjusting the ratio of N<sub>2</sub> and O<sub>2</sub>. The helium flow rate on the tube side was

60 mL/min. The oxygen partial pressure ( $P_{O_2}''$ ) on the tube side can be calculated by using the formula:  $P_{O_2}'' = C_{O_2} \times P_0$  ( $P_0$  is 1.0 atm oxygen pressure). So the oxygen partial pressure ( $P_{O_2}''$ ) is equal to the oxygen concentration ( $C_{O_2}$ ) which can be measured with the GC (HP6890) and the data were acquired under conditions where  $P_{O_2}'$  was varied step by step while the temperature was kept constant and vice versa where the temperature was varied in steps while  $P_{O_2}'$  was kept constant.

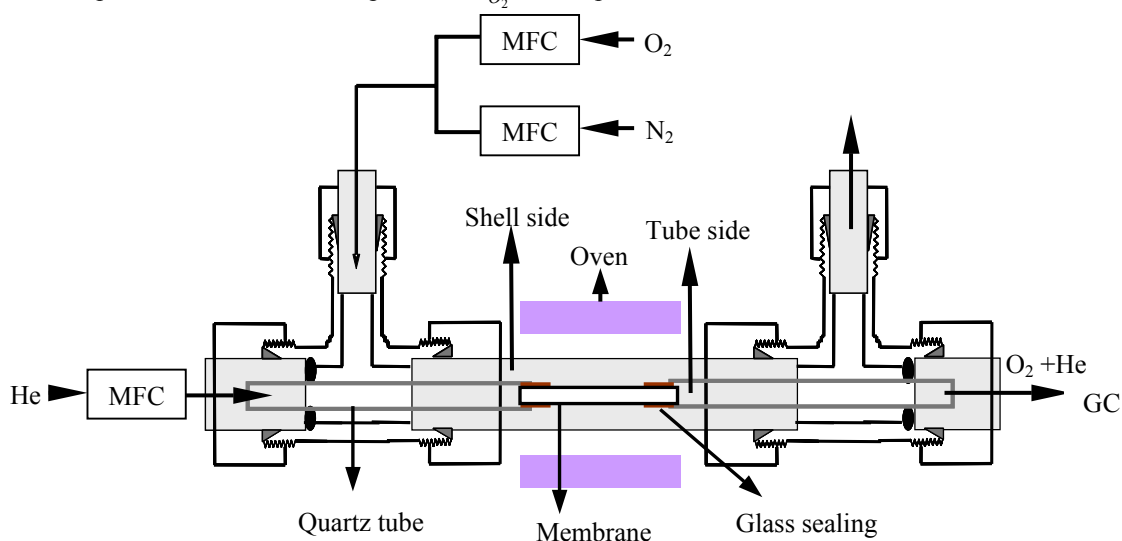


Fig. 3: Schematic diagram of high temperature permeation cell of tubular membrane.

#### 4. Results and Discussion

Fig. 4 gives the oxygen permeation flux through the BSCF membrane tube as a function of the oxygen partial pressure on the shell side at temperatures from 700 °C to 900 °C. As shown in Fig. 4, the oxygen permeation flux increases with increasing oxygen partial pressure on the shell side. The oxygen permeation flux reaches 3.0 mL/cm<sup>2</sup>.min at 900 °C under the oxygen partial pressure of 1.0 atm on the shell side. This result indicates that sufficient oxygen permeation flux demanded for an industrial application can be achieved by increasing the air pressure on the shell side. The oxygen permeation flux increases with increasing temperature, which can be attributed to the increase of the oxygen diffusion with rising temperature.

Figs. 5 and 6 plot the oxygen permeation flux against the oxygen partial pressure terms according to Eqs. (24) and (25), respectively. Fig. 5 shows that there is no linear

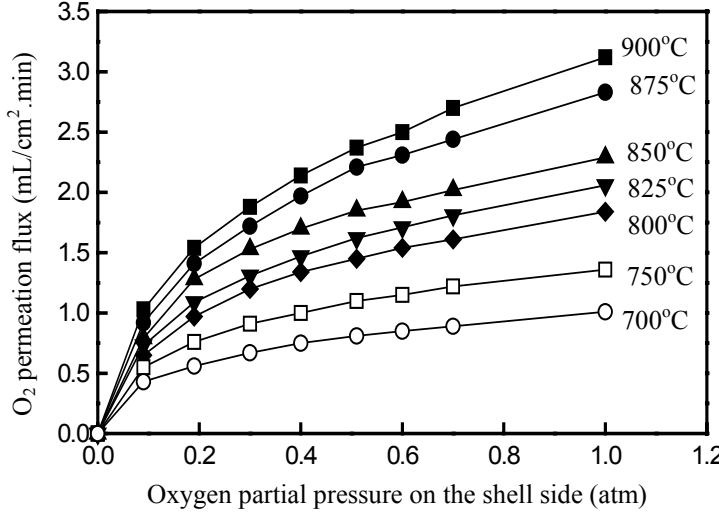


Fig. 4: Oxygen permeation flux through the BSCF membrane tube as a function of the oxygen partial pressure on the shell side.

*Flow rates: a mixture of O<sub>2</sub> and N<sub>2</sub> = 300 mL/min, He = 60 mL/min, P<sub>O<sub>2</sub></sub>' varied from 0.09 atm to 1.0 atm; P<sub>O<sub>2</sub></sub>'' varied from 0.0093 atm to 0.1147 atm. ϕ<sub>2</sub> = 7.96 mm, ϕ<sub>1</sub> = 4.56 mm, L=17.68 mm, S = 2.531 cm<sup>2</sup>.*

relationship between the oxygen permeation flux and  $\left(\sqrt{P_{O_2}' / P_0} - \sqrt{P_{O_2}'' / P_0}\right)$  at the temperature range of 700 °C to 900 °C. However, a linear relationship of the oxygen permeation flux and  $\ln\left(\frac{P_{O_2}'}{P_{O_2}''}\right)$  was found in Fig. 6 at the same temperature ranges.

These phenomena demonstrate that the oxygen transport is limited by the bulk diffusion at the temperature range of 700 °C to 900 °C. We also carried out the experiment about the thickness dependence of the oxygen permeation flux based on the BSCF disk-type membrane, as shown in Fig. 7. Under the same driving force, the oxygen permeation flux ( $J_{O_2}$ ) through the membranes with different thicknesses ( $d$ ) should follow Eq. (26) if the oxygen permeation is completely controlled by the bulk diffusion. Otherwise, it ought to follow Eq. (27) if the oxygen permeation is completely controlled by the surface exchange.

$$\frac{J_{O_2}(d_1)}{J_{O_2}(d_2)} = \frac{d_2}{d_1} \quad (26)$$

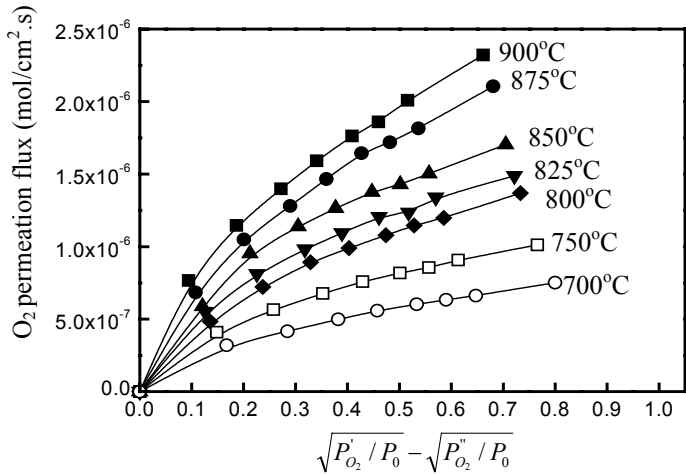


Fig. 5: Oxygen permeation flux through the BSCF membrane tube against  $\left(\sqrt{P_{O_2}^{\prime} / P_0} - \sqrt{P_{O_2}^{\prime\prime} / P_0}\right)$  at different temperatures.

Flow rates: a mixture of  $O_2$  and  $N_2$  = 300 mL/min, He = 60 mL/min,  $P_{O_2}^{\prime}$  varied from 0.09 atm to 1.0 atm;  $P_{O_2}^{\prime\prime}$  varied from 0.0093 atm to 0.1147 atm.  $\phi_2$  = 7.96 mm,  $\phi_1$  = 4.56 mm,  $L$  = 17.68 mm,  $S$  = 2.531  $cm^2$ .

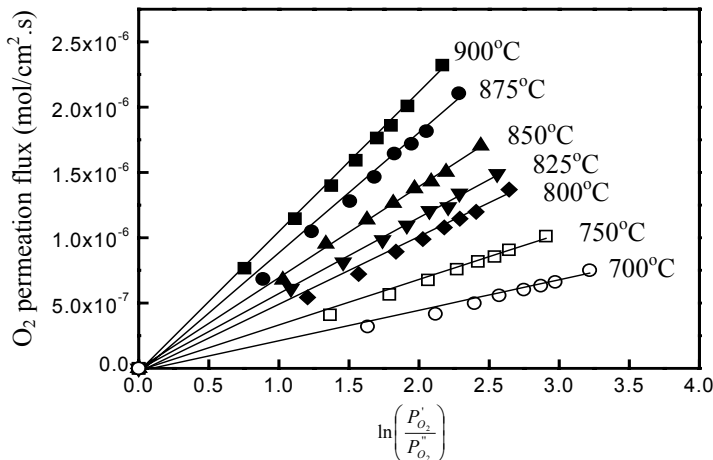


Fig. 6: Oxygen permeation flux through the BSCF membrane tube against  $\ln\left(\frac{P_{O_2}^{\prime}}{P_{O_2}^{\prime\prime}}\right)$  at different temperatures.

Flow rates: a mixture of  $O_2$  and  $N_2$  = 300 mL/min, He = 60 mL/min,  $P_{O_2}^{\prime}$  varied from 0.09 atm to 1.0 atm;  $P_{O_2}^{\prime\prime}$  varied from 0.0093 atm to 0.1147 atm.  $\phi_2$  = 7.96 mm,  $\phi_1$  = 4.56 mm,  $L$  = 17.68 mm,  $S$  = 2.531  $cm^2$ .

$$\frac{J_{O_2}(d_1)}{J_{O_2}(d_2)} = \text{const.} \quad (27)$$

As shown in Fig. 7, the oxygen permeation fluxes through membranes with different thicknesses almost fit Eq. (26). This result indicates that the oxygen permeation was mainly controlled by the bulk diffusion.

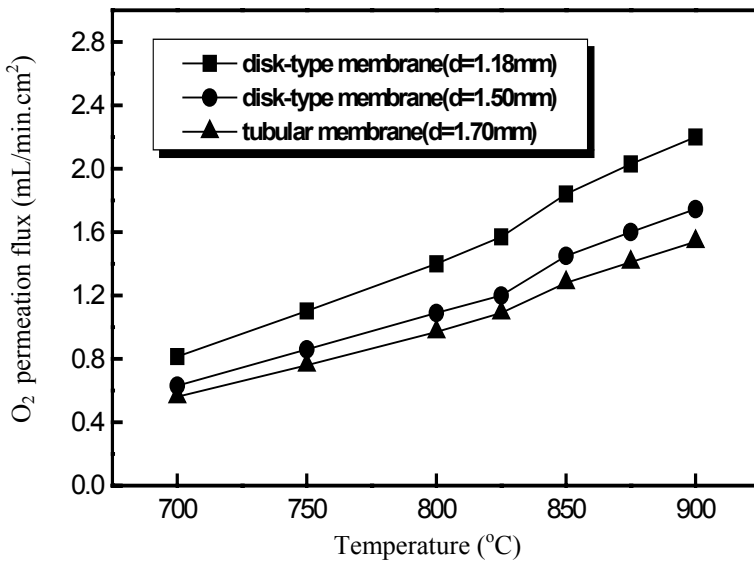
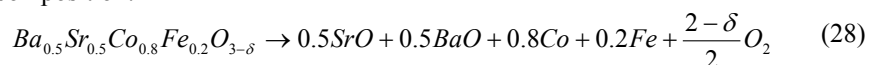


Fig. 7: Temperature dependence of the oxygen permeation flux of BSCF membranes of different thicknesses.

Based on the slopes of the lines in Fig. 6, we can calculate  $D_i$  at the indicated temperatures. The results are shown in Table 1.  $D_v = D_i \times \frac{3-\delta}{\delta}$  was used to convert the measured  $D_i$  value to the oxygen vacancy diffusion coefficient,  $D_v$  [21]. The oxygen content was determined by thermogravimetric analysis. First, the BSCF oxide was pretreated in air with a flow rate of 60 mL/min at 950 °C for 2h to remove the traces of water. After the temperature was decreased to room temperature, a mixture of 5% H<sub>2</sub> and 95% Ar was used to reduce the sample by increasing the temperature to 900 °C at a heating rate of 10 °C/min. The sample was held at 900 °C for 3h to ensure its complete reduction. During the hydrogen reduction, the BSCF underwent the following decomposition:



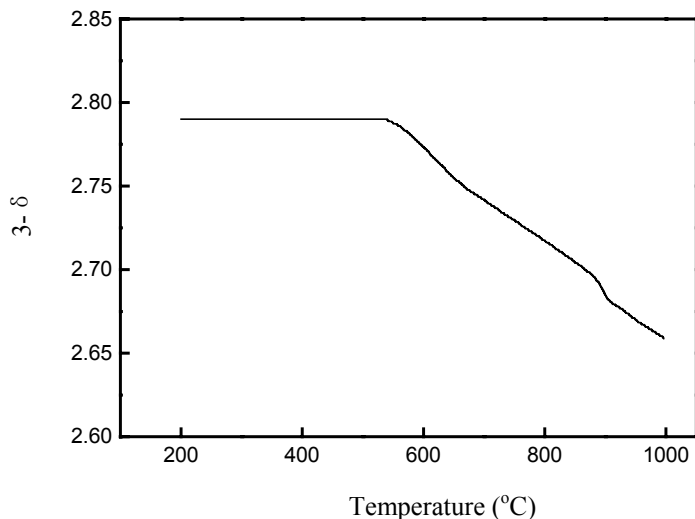


Fig. 8: Development of oxygen vacancy ( $\delta$ ) as a function of temperature as derived from thermogravimetric data for the BSCF oxide in air.

Based on the above equation and the weight loss (13.27%), the oxygen content in the BSCF was calculated to be  $3 - \delta = 2.79$  at room temperature with  $\delta$  as the oxygen vacancy called the oxygen non-stoichiometry. The oxygen content in the BSCF at other temperatures can be determined by a thermogravimetric analyzer. Measurements were carried out up to 1000 °C at a heating rate of 10 °C/min in air with a flow rate of 60 mL/min. The oxygen content at different temperatures can be calculated from the TG curve. As shown in Fig. 8, the oxygen content decreases with increasing temperature.

Therefore, the oxygen vacancy diffusion coefficients  $D_v$  can be calculated from the  $D_i$  and the oxygen content at the different temperatures, the results are also shown in

Table 1 Results of oxygen ion diffusion coefficient ( $D_i$ ), the oxygen content ( $3 - \delta$ ) and oxygen vacancy diffusion coefficient ( $D_v$ ) at different temperatures.

Temperature (°C)	$D_i$ (cm <sup>2</sup> /s)	$3 - \delta$	$D_v$ (cm <sup>2</sup> /s)
900	$3.31 \times 10^{-6}$	2.684	$2.82 \times 10^{-5}$
875	$2.83 \times 10^{-6}$	2.698	$2.53 \times 10^{-5}$
850	$2.34 \times 10^{-6}$	2.704	$2.14 \times 10^{-5}$
825	$1.87 \times 10^{-6}$	2.711	$1.75 \times 10^{-5}$
800	$1.68 \times 10^{-6}$	2.718	$1.62 \times 10^{-5}$
750	$1.16 \times 10^{-6}$	2.730	$1.17 \times 10^{-5}$
700	$0.77 \times 10^{-6}$	2.742	$0.82 \times 10^{-5}$

Table 1. S. Kim et al. [25] determined the  $D_v$  for the  $\text{SrCo}_{0.8}\text{Fe}_{0.2}\text{O}_{3-\delta}$  (SCF) based on the model. The result was in a good agreement with those derived from the isotope exchange measurement. It was found that the corresponding  $D_v$  for the SCF ( $D_v = 1.7 \times 10^{-5} \text{ cm}^2/\text{s}$ , at 890 °C) is higher than that for  $\text{La}_{1-x}\text{Sr}_x\text{CoO}_{3-\delta}$  ( $x = 0$ ,  $D_v = 3.2 \times 10^{-6} \text{ cm}^2/\text{s}$  at 900 °C). The higher  $D_v$  was attributed to the reduction of the repulsive interaction generated from the oxygen vacancy migrating through the saddle point configuration (the triangle defined by two A cations and one B cation) because of the substitution of the smaller  $\text{La}^{3+}$  ion ( $r = 150 \text{ pm}$ ) in A-site by a larger  $\text{Sr}^{2+}$  ion ( $r = 158 \text{ pm}$ ). As expected, we also found that the  $D_v$  ( $D_v = 2.82 \times 10^{-5} \text{ cm}^2/\text{s}$ , at 900 °C) for the BSCF is higher than that for the SCF ( $D_v = 1.7 \times 10^{-5} \text{ cm}^2/\text{s}$ , at 890 °C). The reason is that the substitution of the smaller  $\text{Sr}^{2+}$  ion ( $r = 158 \text{ pm}$ ) in the SCF by the larger  $\text{Ba}^{2+}$  ion ( $r = 175 \text{ pm}$ ) results in the reduction of the repulsive interaction and the increase in the mobility of the oxygen vacancy.

### Conclusion

As an example for atomic oxygen transport in oxide crystals, we have provided a study devoted to the oxygen permeation flux through the BSCF perovskite membrane tube. Fluxes were determined at different oxygen partial pressures on the shell side and different temperatures between 700 °C and 900 °C. The permeation rate of the BSCF perovskite membrane was found to be controlled between 700 °C and 900 °C by the bulk diffusion rather than by the surface process. This conclusion is in complete agreement with the experimental finding from measuring oxygen permeation through membranes of different thickness. The oxygen vacancy diffusion coefficients ( $D_v$ ) of the BSCF perovskite membrane at different temperatures were calculated from the dependence of the oxygen permeation flux on the oxygen partial pressure based on the surface exchange fluxes model.

### Acknowledgement

H. Wang greatly thanks the Alexander von Humboldt Foundation for the financial support.

### References

- [1] T. He, Q. Huang, A. P. Ramirez, Y. Wang, K. A. Regan, N. Rogado, M. A. Hayward, M. K. Haas, J. S. Slusky, K. Inumara, H. W. Zandbergen, N. P. Ong, R. J. Cava, *Nature* 54 (2001) 411.
- [2] Y. Xu, C. McCammon, B.T. Poe, *Science* 282 (1998) 922.
- [3] D. D. Fong, G. B. Stephenson, S. K. Streiffer, J.A. Eastman, O. Auciello, P. H. Fuoss, C. Thompson, *Science* 304 (2004) 1650.
- [4] J. Junquera, P. Ghosez, *Nature* 422 (2003) 506.
- [5] C. C. Homes, T. Vogt, S. M. Shapire, S. Wakimoto, A. P. Ramirez, *Science* 293 (2001) 673.

- [6] Y. Moritomo, A. Asamitsu, H. Kuwahara, Y. Tokura, *Nature* 380 (1996) 141.
- [7] Y. Teraoka, T. Nobunaga, N. Yamazoe, *Chem. Lett.* 195 (1988) 503.
- [8] H. H. Wang, Y. Cong, W. S. Yang, *J. Membr. Sci.* 210 (2002) 259.
- [9] U. Balachandran, J. T. Dusek, P. S. Maiya, B. Ma, R. L. Mieville, M. S. Kleefish, C. A. Udovich, *Catal. Today* 36 (1997) 117.
- [10] H. H. Wang, Y. Cong, W. S. Yang, *Catal. Today* 82 (2003) 157.
- [11] C. Y. Tsai, A. G. Dixon, W. R. Moser, Y. H. Ma, *AIChE J.* 43 (1997) 2741.
- [12] H. H. Wang, Y. Cong, W. S. Yang, *Chinese Science Bulletin* 47 (7) (2002) 534.
- [13] S. Xu, W. J. Thomson, *AIChE J.* 43 (1997) 2731.
- [14] H. H. Wang, Y. Cong, W. S. Yang, *Chem. Comm* 14 (2002) 1468.
- [15] F. T. Akin, Y. S. Lin, *J. Membr. Sci.* 209 (2002) 457.
- [16] H. H. Wang, Y. Cong, W. S. Yang, *Catal. Lett.* 84 (2002) 101.
- [17] H. H. Wang, Y. Cong, X. F. Zhu, W. S. Yang, *React. Kinet. Catal. Lett.* 79 (2003) 351.
- [18] F. T. Akin, Y. S. Lin, *Catal. Lett.* 78 (2002) 239.
- [19] H. Wang, Y. Cong, W. Yang, *Catal. Today* 104 (2005) 160
- [20] R. J. Chater, S. Carter, J.A. Kilner, B.C.H. Steele, *Solid State Ionics*, 53-56 (1992) 85
- [21] A. Thursfield, I. S. Metcalfe, *J. Mater. Chem.*, 14 (2004) 2475
- [22] Z. P. Shao, W. S. Yang, Y. Cong, H. Dong, J. H. Tong, G. X. Xiong, *J. Membr. Sci.* 172 (2000) 177.
- [23] C. G. Guizard, A. C. Julbe, in: *Recent Advances in Gas Separation by Microporous Ceramic Membranes*, part VI, (ed. by N.K. Kanellopoulos), Elsevier (2000) , pp. 435-471
- [24] H. J. M. Bouwmeester, A. J. Burggraaf, in: *Fundamentals of Inorganic Membrane Science and Technology* (eds. A.J. Burggraaf and L. Cot), Elsevier, (1996), pp.435-528
- [25] S. Kim, Y. L. Yang, R. Christoffersen, A. J. Jacobson, *Solid State Ionics*. 109 (1998) 187.
- [26] S. Kim, Y. L. Yang, A. J. Jacobson, B. Abeles, *Solid State Ionics*. 106 (1998) 189.
- [27] H. H. Wang, Y. Cong, W. S. Yang, *J. Membr. Sci.* 209 (2002) 143.